Pergamon

0301-9322(95)00043-7

Int. J. Multiphase Flow Vol. 21, No. 6, pp. 963–984, 1995

0301-9322/95 $9.50 + 0.00

HEAT TRANSFER ENHANCEMENT BY A PARTICLE ON THE BOTTOM OF A FLUME

G. HETSRONI, R. ROZENBLIT and D. M. LU

Faculty of Mechanical Engineering, Technion, Israel Institute of Technology, Haifa, Israel

(Received 17 August 1994; in revised form 2 May 1995)

Abstract—Infrared thermography was used to study the effect of a spherical particle on the local heat transfer from a heated plate. The measurement of the temperature field with the particle and without it showed that the heat transfer coefficient increased locally by a factor of 1.5–3, for a particle of the order $d_p^+ = 10$-25. A general decrease in the wall temperature was observed in the region under and in front of the particle. No effect of the particle material was noted. The temperature fluctuations at a point on the heated plate were also studied. These fluctuations are related to the bursting process in the turbulent flow. The bursting period increased by 60–70% for the flow near the particle, whereas the root mean square of the temperature fluctuations decreased up to 2.5 times. This may mean that the heat transfer enhancement is governed by a mechanism other than the change in the turbulence structure. Numerical computations of the flow field near the spherical particle were performed. These clearly indicate that fluid from the mainstream is directed towards the bottom of the flume, in front of the particle, thus cooling the heated surface. One can conclude that the change in the velocity profile near the wall caused by the particle is the reason for the local heat transfer enhancement.

Key Words: heat transfer enhancement, two-phase flow, particles, thermography

1. INTRODUCTION

In the studies by Hetsroni & Rozenblit (1994), using infrared thermography, it was established that there exists an interaction between particle-laden turbulent flow and a heated plate. We noted also that a change in the particle loading or the particle dimension, changed the value of the heat transfer coefficient. Similar conclusions on the heat transfer coefficient were drawn by others. Plass & Molerus (1974) found that for a given suspension liquid flow, the increase of heat transfer was strongly dependent on the particle size. Later Zisselmar & Molerus (1979) showed that the solid particles increased or damped the intensity of turbulence, depending on the concentration of solids as well as on the distance from the wall. They noted that the strongest increase in turbulence was observed in the same range of concentration of solids where the maximum heat transfer was achieved.

The effect of the addition of solid particles on the heat transfer in turbulent gaseous flows has been studied by many investigators such as Jepson *et al.* (1963), Wilkinson & Norman (1967) and, more recently, Hasegawa *et al.* (1983). The heat transfer from a tube or an array of tubes in suspension cross flow has been studied, for example, by Murray & Fitzpatrick (1991) for a staggered array of tubes. Investigations in gas flow showed (Murray 1994) that the modification of the heat transfer coefficient is determined by the altered thermal capacity of the mixture, change in the boundary layer velocity profile, an increase in turbulence intensity associated with wake formation by individual particles or turbulence suppression as a result of eddy–particle interactions.

Changes in the boundary layer were observed by Fitzpatrick *et al.* (1992). This took the form of boundary layer thinning over the sides of a tube in a suspension cross flow. Han *et al.* (1991) noted that at low mass loadings in a pipe flow the thickness of the viscous sub-layer is the most significant parameter whereas at higher particle loadings the thermal capacity and conductivity of the mixture are more important. However, heat transfer decreased at a very high particle concentration on the bottom of a water flume (Hetsroni & Rozenblit 1994). This decrease in heat transfer was caused by a build-up of particle dunes, and consequently an increase of the thermal resistance from the heated wall to the water.

Rogers & Eaton (1989) measured the response of solid particles in a vertical boundary layer in air, using a low concentration of 50 and 90 μm glass particles. They found that the RMS velocity fluctuations of both particle sizes nearly equalled the streamwise turbulence intensity of the flow, but

the particle velocity fluctuations in the normal direction was strongly attenuated, i.e. they were much lower than the fluid's. The power spectra of particle velocities showed that for the normal fluctuations the power spectrum shifted to higher frequencies relative to the streamwise fluctuations, therefore indicating that the particles did not closely follow the fluid fluctuations in the normal direction. Rogers & Eaton also used 70 μm copper particles to create a greater particle mass loading of 20%. The presence of these particles tended to suppress turbulence, with the degree of turbulence suppression being a function of the distance downstream in the boundary layer. They attributed the turbulence suppression to an increase in the dissipation. However, they were unable to clarify their results in the light of the observed dominant flow events near the wall. Hetsroni (1989) noted that the presence of solid particles in flow may reduce the turbulence level as a result of eddy–particle interactions, or may enhance turbulence due to wakes and vortex shedding.

In the flow-visualization studies by Kline *et al.* (1967) and later by Kim *et al.* (1971), it was established that there are low and high-velocity streaks in the near-wall region of a bounded turbulent flow and ejections of the low-velocity fluid to the bulk flow. The total ejection process was called a 'burst' by Kim *et al.* (1971). Hetsroni & Rozenblit (1994) noted that particles generally accumulate in the warmer regions of the heated plate, i.e. in the low velocity streaks. A similar conclusion was drawn, without heat transfer, by others such as Rashidi *et al.* (1990), Kaftori *et al.* (1992), Eaton & Fessler (1994) and computed by Pedinotti *et al.* (1992).

Grass *et al.* (1991) studied the effect of the bed roughness condition on the spanwise structure of the near-wall turbulence. This was achieved by using a range of different diameters (d_p = 1.15, 6 and 12 mm) of glass spheres, randomly packed in a single layer, resting on a glass bed plate. Preliminary results showed that, just as in the case of viscous sublayer region of smooth wall flow, a dominant spanwise wavelength occurs in the instantaneous crossflow distribution of streamwise velocity close to the rough wall. The measurements indicated that for fully rough wall conditions, this wavelength is directly proportional to the bed roughness size.

At present there is a disagreement about the value of the dimensionless time interval between bursts $\Delta\tau^+ = \Delta\tau u^{*2}/\nu$ (here $\Delta\tau$ is the time interval between bursts, u^* is the shear velocity and ν is the fluid viscosity), even in a clear fluid.

Several methods have been used to detect this interval from turbulent measurements. In studies by Wallace *et al.* (1972) the motions of the fluid were analyzed in the four quadrants of the (u, v)-plane. Lu & Willmarth (1973) later extended this method by employing a threshold level. However, the variable interval time averaging (VITA) technique, developed by Blackwelder & Kaplan (1976), is perhaps the most widely used detection method. These detection algorithms are very sensitive to the values of the sampling criteria so that a given fractional change in the threshold may produce a fractional change of the same order in some of the final statistics. Blackwelder & Haritonidis (1983) suggested that in the VITA and other detection techniques, almost any value of short-time variance could have been obtained by choosing various values of the threshold. However, the threshold K and averaging time T significantly affect the bursting frequency as detected by the VITA technique, and the choice of K and T is always controversial.

Blackwelder & Kaplan (1976) used the value $T^+ = Tu^{*2}/\nu = 10$ and $K = 1.0$–1.2 to deduce bursting frequency in turbulent boundary-layer flow. Blackwelder & Haritonidis (1983) found that an average interval between bursts of typically $\Delta\tau = 300\nu/u^{*2}$ is constant over the Reynolds number range $10^3 < \mathrm{Re}_\theta < 10^4$ (here $\mathrm{Re}_\theta = u_\infty\theta/\nu$, where θ is the momentum boundary layer thickness, u_∞ is the mean velocity and ν is the fluid's viscosity). Blackwelder & Eckelmann (1978) used the same detection process and parameters in an oil channel. Their data yielded $\Delta\tau^+ = 250$ at $y^+ = 15$ and $\mathrm{Re}_\theta = 400$ (here $y^+ = yu^*/\nu$, where y is the distance from the wall, $u^* = \sqrt{\tau/\rho}$ is the shear velocity, τ is the shear stress at the wall and ρ is the fluid's density). The data of Willmarth & Sharma (1984) have shown that the burst period, scaled with the viscous timescale, was about $\Delta\tau^+ \cong 350$ independent of the Reynolds number. The experiments were carried out in a wind-tunnel facility at Reynolds numbers $\mathrm{Re}_\theta = 6480$ and $\mathrm{Re}_\theta = 9840$. Hatziavramidis & Hanratty (1979) summarized measurements of spectra of the fluctuations of the wall velocity gradient in pipe flows. It was found that the median bursting period was $\Delta\tau^+ \cong 110$. The visual measurements of the bursting frequency summarized by Kim *et al.* (1971) gave a median bursting period of $\Delta\tau^+ \cong 100$ in close agreement with the median frequency of the velocity fluctuations. In the study carried out by Luchik & Tiederman (1987) burst-detection schemes were developed and it was shown that the bursting events were closely

correlated with fluid moving both away from the wall and toward the wall. The average time between bursts, normalized with inner variables and determined by using the various probe techniques, was $\Delta\tau^+ \cong 90$. Kaftori *et al.* (1994) report that the average non-dimensional time between funnel vortices was $\Delta\tau^+ = 91.5$ and was in agreement with Luchik & Tiederman (1987) and Rashidi & Banerjee (1988) who reported a value of 85.

Our measurements of the thermal signals on the wall shed some additional light on this

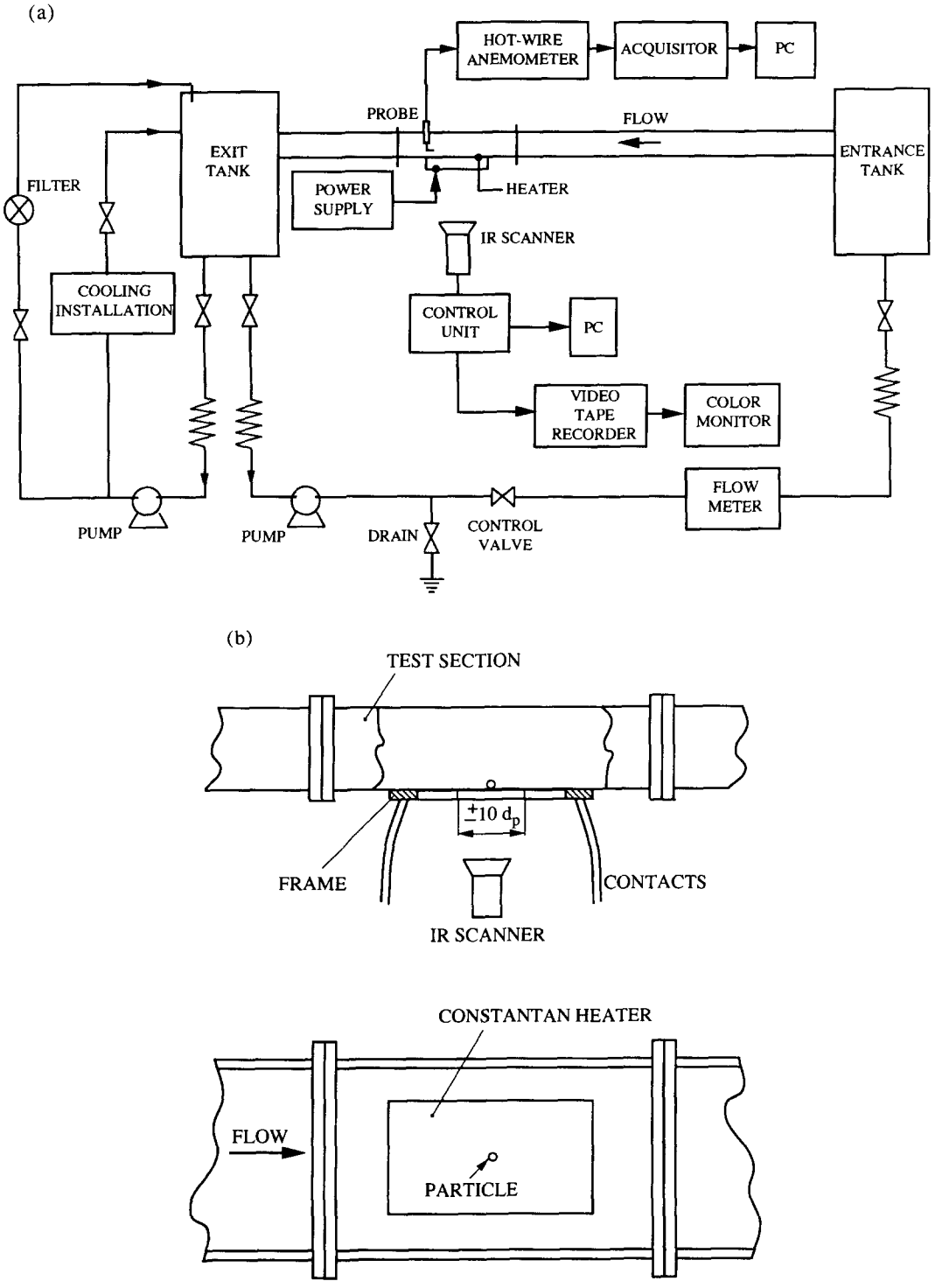

Figure 1. (a) The experimental set-up. (b) The cross section of the heater, with the spherical particle.

Table 1. Flow conditions

Mean velocity U_m (cm s^{-1})	Mean temperature of water t_L (°C)	Flow depth h (cm)	Reynolds number $Re_h = U_m h/\nu$	Friction velocity u^* (cm s^{-1})	Particle motion
7.8	20 ± 0.2	6.7	5150	0.45	no
13.0	20	6.7	8650	0.7	no

Table 2. Particle characteristics

Particle material	Diameter (mm)	Specific gravity (g cm^{-3})	Particle geometry
Steel	2.40	7.9	spherical
	4.75	7.9	spherical
Glass	4.3	2.52	spherical
	1.2	2.52	spherical

phenomenon and allows us to estimate the effect of the particle on the turbulence structure, as shown below. We also aim to clarify the mechanism which causes an increase in the heat transfer coefficient, when the particle loading is light. We do so by studying the non-stationary thermal field of the heated plate near a single, stationary, spherical particle. We have chosen a stationary particle since one knows where the particle is in space, at any given time, and since the relative velocity between the particle and the fluid is maximal.

2. EXPERIMENTAL

2.1. Experimental facility and measurement technique

The experimental facility and measurement technique were described in detail in Hetsroni & Rozenblit (1994). Therefore, we present only the main properties here. The loop is a stainless steel open flume, 4.3 m long, 0.32 m wide and 0.1 m deep. Water of constant temperature was recirculated in it, with the flow rate being measured by means of a flowmeter. The constantan heater is located at the bottom of the test section. It is a strained (on an insulated frame) foil, 0.33 m long, 0.2 m wide and 50 μm thick. The window of the frame is 0.3 m long and 0.15 m wide (figure 1). The foil is attached to the window by means of contact adhesive and is coated on the air side with black matt paint of about 20 μm thickness. A constant heat flux of $q = 1.01$ W cm^{-2} is achieved by supplying d.c. power up to 300 A.

The non-stationary temperature distribution at the heater surface is measured by using an I.R. imaging radiometer. The temperature range of the radiometer is -20 to 1500°C, with a minimum detectable temperature difference of 0.1°C at 30°C. Through calibration, the thermal imaging radiometer is very accurate in a narrow temperature range, giving typical noise equivalent temperature difference (NETD) only, which is less than 0.2°C (with image average less than 0.05°C). A typical horizontal resolution is 1.8 mRad or 256 pixels/line.

2.2. Experimental conditions and procedures

A fully developed flow was established in the region beyond 2.5 m downstream from the entrance to the flume, which was confirmed by measuring the velocity distribution. The studies of thermal field

Table 3. Typical uncertainty estimates

Variable	Uncertainty
t_L	0.05°C
t_w	0.15°C
$\bar{t}_w$	0.05°C
U_m	2%
u^*	5.5%
$\Delta\tau^+$	12.2%
d_p	0.5%

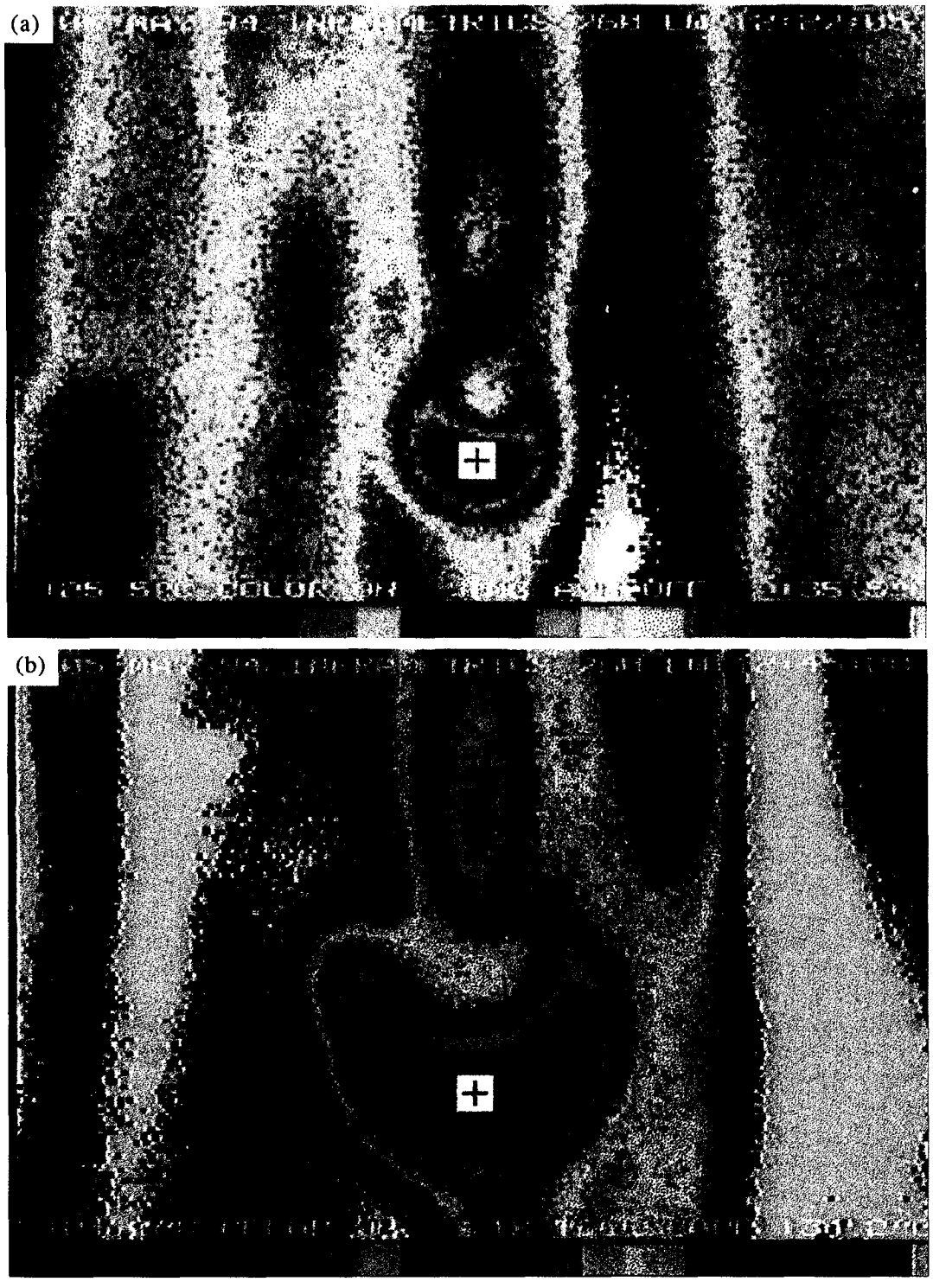

Figure 2. The thermal field of the heated foil near the spherical particle. $Re_h = 8650$, the particle diameter is (a) $d_p = 0.24$ cm; $d_p^+ = 17$, (b) $d_p = 0.475$ cm; $d_p^+ = 33$. Flow direction is from the bottom to the top. The dimensionless width of the figure is $\Delta z^+ = 250$.

of the heater plate were carried out at two values of Reynolds numbers $Re_h = 5150$ and $Re_h = 8650$ (here $Re_h = U_m h/\nu$, where U_m is the mean velocity, h is the water level and ν is the fluid viscosity).

A hot film anemometer, with a standard single-sensor boundary-layer probe, was used for measurements of the mean velocity profile. The probe was connected to a traversing mechanism having a spatial resolution of 10 μm. The anemometer signal was transmitted in digital code through an acquisition system to a PC. The streamwise velocity profiles were then employed to determine values of the friction velocity u^*, by means of 'Clayser-type' fits.

During this investigation a single particle was placed (motionless) on the heated foil. The particle was situated at a distance of 0.18 m from the leading edge of the heater, at the center-line of the flume. In these experiments we used particles with high specific gravity and relatively large diameter. The values of flow parameters used in this study are listed in table 1. Particle characteristics are listed in table 2.

The study of the local heat transfer coefficient around the motionless particle on the heated wall was done in the following way. We placed the scanner of the I.R. radiometer under the heater plate, at a distance of about 0.5 m, and measured the temperature at various points along the central line of the heater. These measurements were carried out both with the particle and without it. This was done in order to eliminate the influence of the heater temperature field on the results. For the quantitative analysis we use the 'Point mode' of the I.R. radiometer, i.e. the temperature at each point is digitized and transmitted to be stored on a PC. During each run, a sequence of at least 200 s was recorded. The sampling time was 0.05 s. Both the average temperature at the point and the RMS temperature fluctuations within each run were examined. Simultaneously, the thermal pattern was recorded on a video cassette. The video was then used in a playback mode to analyze the data, i.e. to determine the influence of the particle on the pattern of the thermal streaks.

The uncertainty caused by equipment inaccuracy and statistical variations was estimated and are listed in table 3.

3. EXPERIMENTAL RESULTS

3.1. Local heat transfer coefficient near the motionless particle

We (Hetsroni & Rozenblit 1994) have shown previously that the thermal field on the air side of the heated foil is almost the same as the temperature pattern on the bottom of the flume (i.e. on the water side of the heated foil). A distortion in the measured values of the temperature fluctuations begins at characteristic frequencies higher than 15 Hz. Below this frequency, the distortion is less than 1%. In this investigation we observed characteristic frequencies of about 0.1–0.2 Hz.

Figure 2 depicts the typical instantaneous thermal field of the heated foil near the location of the particle. The color shades are proportional to the temperature, and thus reveal the colder region in front and under the motionless particle. In the wake of the particle, a region of higher temperature (i.e. the zone with the lower velocity) can be seen. At a distance of a few diameters after the particle, we observe a region with lower temperature, that probably corresponds to the mixing zone.

For the definition of the local heat transfer coefficient, we used the time averaged temperature at a measuring point. The relative average local heat transfer coefficient is defined at corresponding points as:

$$\frac{\alpha_p}{\alpha_{wp}} = \frac{(\bar{t}_{wp} - t_L)}{(\bar{t}_p - t_L)} \qquad [1]$$

here α_p is the average local (at a point) heat transfer coefficient (wall to fluid) when the particle is present, α_{wp} is the average local heat transfer coefficient at the corresponding point without the particle, $\bar{t}_p$ is the time-average temperature at a point on the wall when the particle is present, $\bar{t}_{wp}$ is the time-average temperature at the corresponding point without the particle and t_L is the liquid bulk temperature, which was kept constant during each run.

Figure 3 depicts the variation of the value α_p/α_{wp} versus the dimensionless streamwise distance x/d_p (here x is the streamwise distance from the particle location and d_p is the particle diameter) at Reynolds number $Re_h = 5150$. The curves display maxima, with the maximum value increasing with increasing particle diameter. It can be seen that the maxima are shifted to the left with the increasing

diameter of the particle. This tendency is demonstrated in figure 4, where the variation of the relative local heat transfer coefficient α_p/α_{wp} is shown versus the dimensionless streamwise coordinate $x^+ = xu^*/\nu$ from the location of the particle.

We also observed an increase in the relative local heat transfer coefficient as the Reynolds number increases (figure 5). In this figure, one can also observe some heat transfer enhancement at the wake of the particle at $Re_h = 8650$.

3.2. Temperature fluctuations at the wall

While flow-visualization studies have provided useful information about coherent structures in turbulent flows, most of the quantitative information has been gained by the use of conditional sampling and averaging techniques. The wide scatter in the results indicates that the number of bursts detected per unit time varies significantly, depending on which detection algorithm is used. Here we used the variable interval time averaging (VITA) technique, developed by Blackwelder & Kaplan (1976). This technique is perhaps the most widely used detection method.

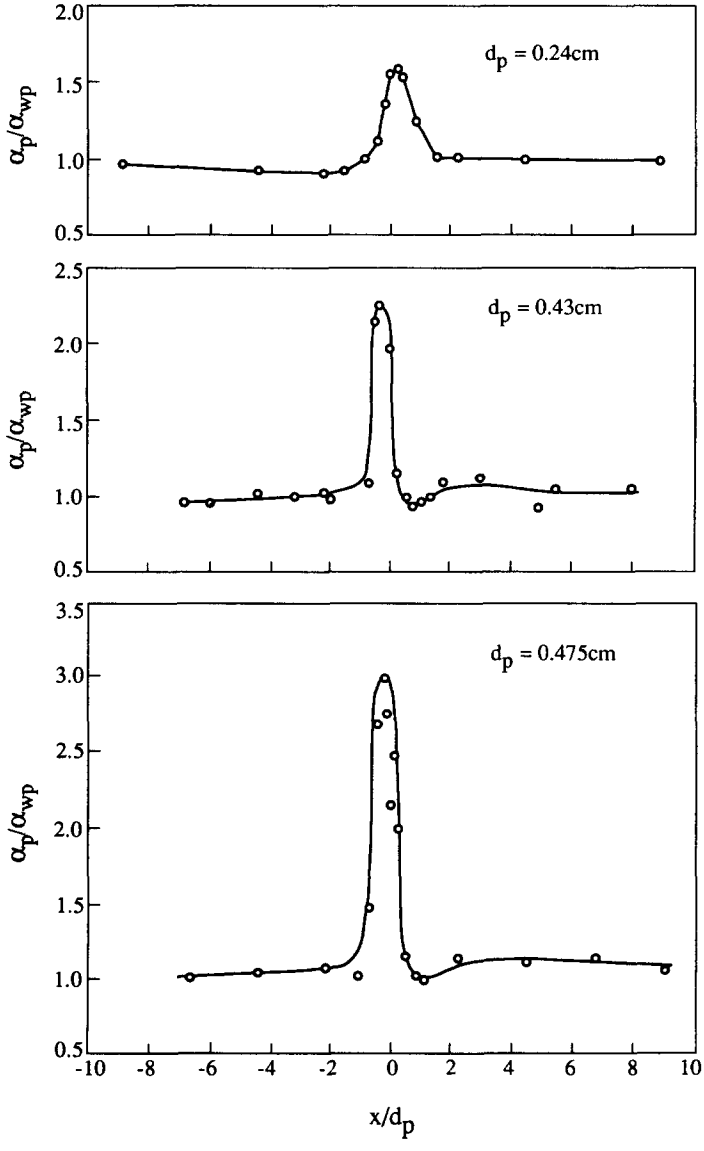

Figure 3. Variation of the value of the local relative heat transfer coefficient α_p/α_{wp} vs the dimensionless streamwise distance x/d_p at $Re_h = 5150$.

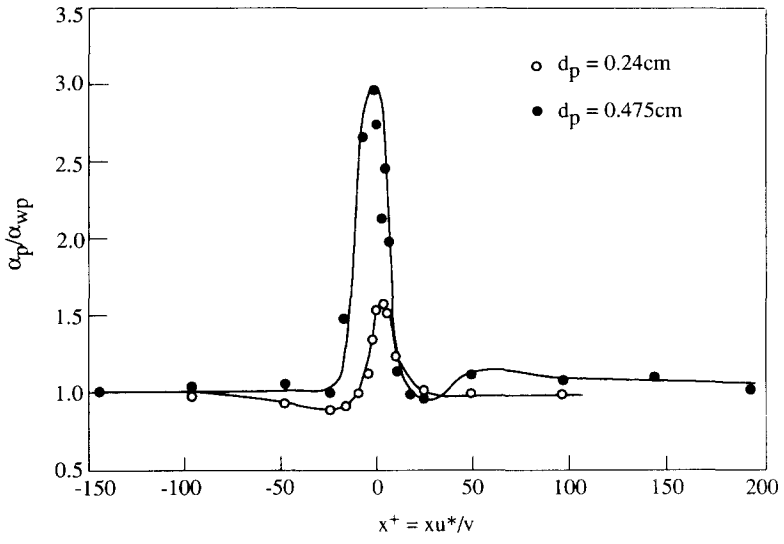

Figure 4. Variation of the relative local heat transfer coefficient α_p/α_{wp} vs the dimensionless streamwise distance $x^+ = xu^*/\nu$ from the particle. $Re_h = 5150$.

The variable interval time average (VITA) of a fluctuating quantity $\theta(\tau) = t(\tau) - \bar{t}$ is defined as:

$$< \theta(\tau,T) > = \frac{1}{T}\int_{\tau-\frac{1}{2}T}^{\tau+\frac{1}{2}T} \theta(\tau)\,d\tau \qquad [2]$$

where $t(\tau)$ is the instantaneous temperature at a point, $\bar{t}$ is the conventional time average temperature, T is the averaging time and τ is time. This average $< \theta(\tau,T) >$ is effectively a low-pass filter, having zero phase shift, applied to the original function.

In order to obtain a local average of some phenomenon, the averaging time T must be of the order of the time scale of the phenomenon under study.

The localized VITA variance of $\theta(\tau,T)$ is defined as

$$\mathrm{var}(\tau,T) = \langle\theta^2\rangle - \langle\theta\rangle^2 \qquad [3]$$

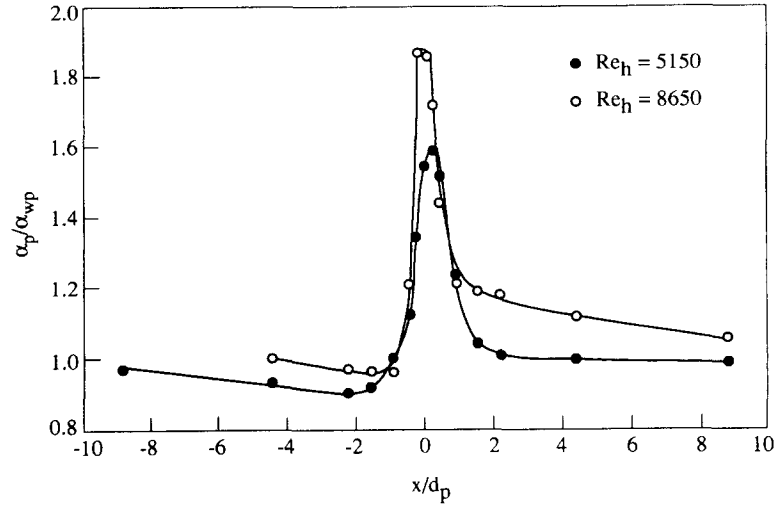

Figure 5. The increase of the relative local heat transfer coefficient for two Reynolds numbers, $d_p = 0.24$ cm.

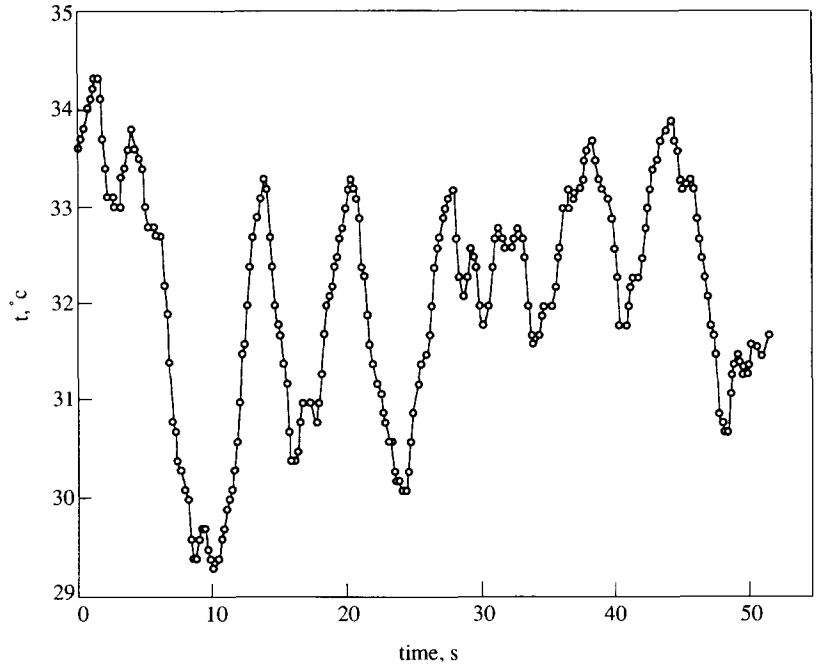

Figure 6. Part of a thermal oscillogram, at a point, with $Re_h = 8650$.

Using this variance, a detection function $D(\tau)$ is defined as

$$D(\tau) = \begin{cases} 1 \text{ if var } > k \cdot \theta'^2_{RMS} \\ 0 \text{ otherwise,} \end{cases} \quad [4]$$

where k is the threshold level and θ'_{RMS} is the conventional root mean square of the total record of the signal $\theta(\tau)$. The number of intervals in which $D(\tau) = 1$ is assumed to give the number of bursts.

The most fundamental question to be addressed by any detection algorithm is whether the signal characteristics used for the detection are actually unique characteristics of an ejection or a burst. Lu & Smith (1991) categorized the types of burst-patterns and compared them with the associated visualization sequences. A detection criterion employing the VITA parameter was used to establish averaged bursting periods, based on the threshold criteria of $k = 1$ and $\delta u/\delta\tau > 0$. Using this approach, the averaged bursting periods for the locations $y^+ = 15$ and $y^+ = 30$, at $Re_\theta = 1520$, were $\Delta\tau^+ = 258$ and 272, respectively, which is close to the bursting period suggested from the probe-rake results of Blackwelder & Haritonidis (1983). Lu & Smith (1991) noted that, if the threshold criteria of $k = 0.4$ and $\delta u/\delta\tau > 0$ were applied, similar to the approach employed by Luchik & Tiederman (1987), the averaging bursting time at detection points $y^+ = 15$ and $y^+ = 30$, for the same data set, decreased to $\Delta\tau^+ \cong 80$, which is comparable to the $\Delta\tau^+ \approx 90$ suggested by Luchik & Tiederman (1987).

Komori *et al.* (1989) adapted a simple sine-wave model to search for an appropriate value of $\Delta\tau$. The numerical calculations by the model showed that an averaging time comparable to the duration of a bursting event should be recommended.

Subramanian *et al.* (1982) found that the VITA scheme, applied to a temperature signal in a slightly-heated boundary layer, corresponded well with the data observed by Chen & Blackwelder (1978).

In figure 6 is shown a typical part of the oscillogram of temperature at the point. These oscillograms were employed to determine the fluctuating and mean values at various points.

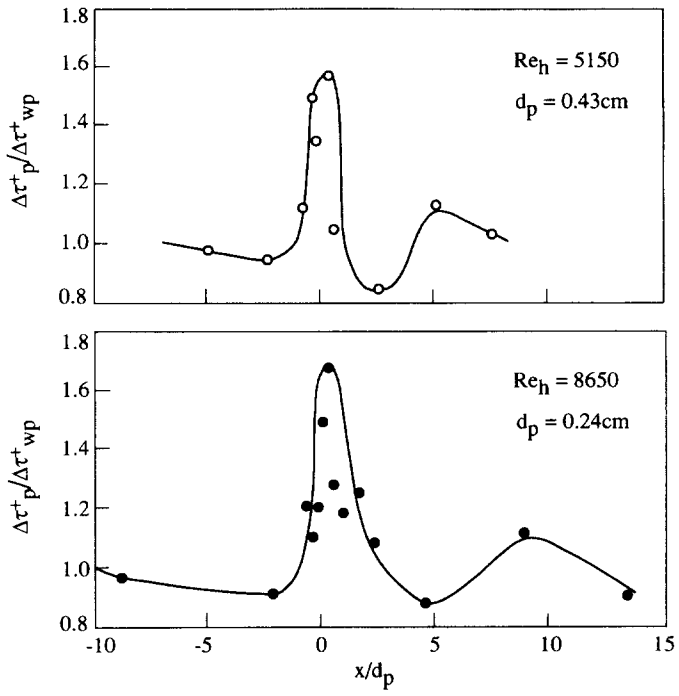

Figure 7. Variation of the dimensionless time between bursts vs dimensionless distance x/d_p.

The VITA analysis of the thermal signal shows:

(1) It is impossible to obtain the results by using the averaging time $T^+ = 10$ and the threshold $k = 1.0$ that were used, for example, by Blackwelder & Kaplan (1976), Blackwelder & Haritonidis (1983) and Blackwelder & Eckelmann (1978).

(2) Using an average time which is comparable with the duration of a bursting event (approximately 1/2 of the time between the bursts, as was recommended by Komori *et al.* 1989) results in stable data. We used $T^+ = 150$ as half a bursting period $\Delta\tau^+ \cong 300$ as in the studies by Blackwelder & Haritonidis (1983) or by Willmarth & Sharma (1984) and the value of the threshold $k = 0.4$, as did Lu & Smith (1991). We obtained the mean bursting period $\Delta\tau^+ = 290$. These data were along the streamwise direction without a particle at Reynolds numbers $Re_h = 5150$ and $Re_h = 8650$. They demonstrated high stability with respect to the change of values of parameters in the range of $0.3 < k < 1.0$.

(3) The presence of the particle on the wall changed the bursting period close to the particle. In figure 7 it is seen that at a distance $\pm 2d_p$ the bursting period increased by 60–70%.

Further analysis of the wall temperature is aimed at defining connections between the temperature fluctuation level and the heat transfer coefficient value.

In figure 8 is shown the distribution of dimensionless RMS temperature RMS_{wp}/Dt_{wp} along

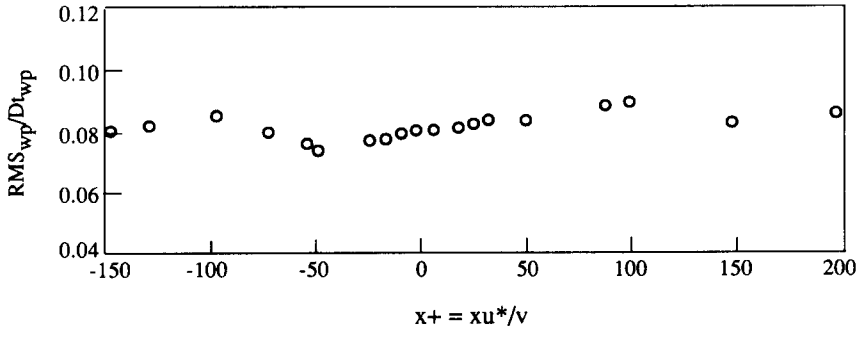

Figure 8. The dimensionless RMS temperature RMS_{wp}/Dt_{wp} in the streamwise direction $x^+ = xu^*/\nu$, $Re_h = 5150$.

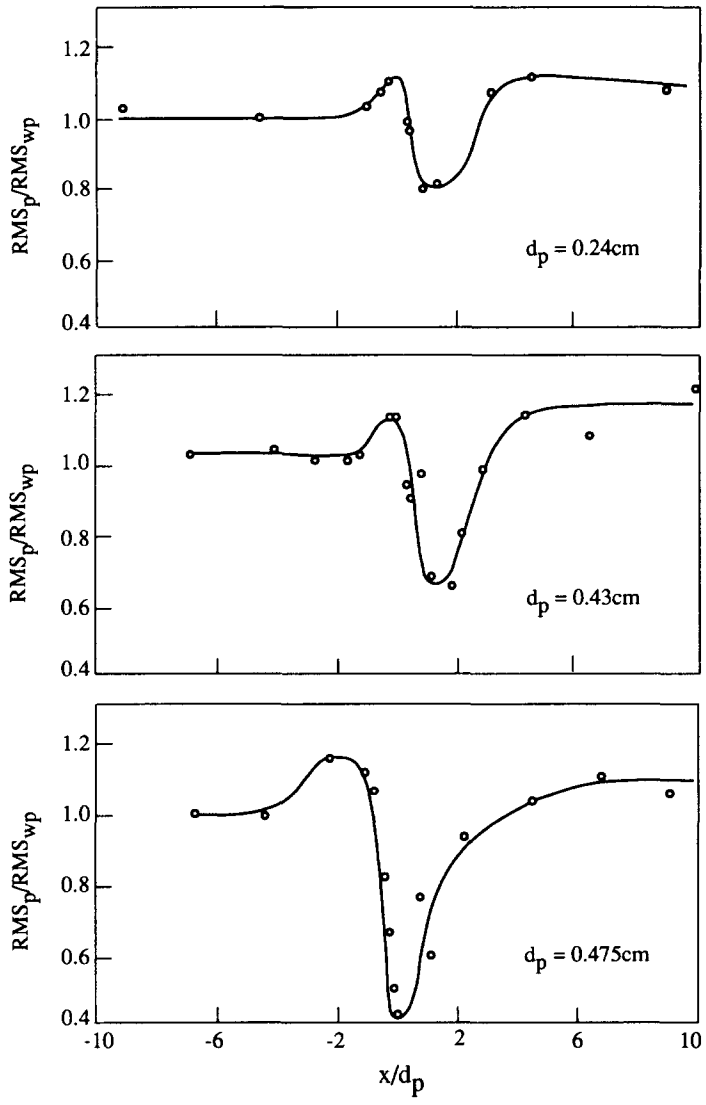

Figure 9. Change of the temperature fluctuation level RMS_p/RMS_{wp} vs the dimensionless distance x/d_p, $Re_h = 5150$.

the streamwise direction x^+. Here RMS_{wp} is the root mean square of the wall temperature fluctuations and Dt_{wp} is the difference between the temperatures of the wall, at a given point, and the bulk liquid temperature (without particle). It is clear from this figure that the value of the dimensionless (RMS_{wp}/Dt_{wp}) generally has a value of ~9% at Reynolds number $Re_h = 5150$. In figure 9 is shown the change of the temperature fluctuation level (RMS_p/RMS_{wp}) along the streamwise direction (here RMS_p and RMS_{wp} are the root mean squares of the wall temperature fluctuations with and without a particle, respectively.) It can be seen that the curves have minima, the values of which increase with the increase in the particle diameter. The minima are shifted to the left with the increase of particle diameter in a manner similar to the shift of curves of the heat transfer coefficient.

These results can be presented as a function of the dimensionless relative RMS temperature $(RMS_p/Dt_p)/(RMS_{wp}/Dt_{wp})$ versus the dimensionless streamwise distance x/d_p (figure 10). Here, we observe the decisive similarity of this graph to the graph of the relative heat transfer enhancement (figure 3).

Figure 11 shows the variation of the maxima of the local heat transfer coefficient as a function of dimensionless particle diameter. This function is monotonous and increases in the range of $5 \leqslant d_p^+ \leqslant 25$.

4. NUMERICAL SIMULATION

Numerical simulation is performed in order to better understand the mechanisms which give rise to the specific heat transfer mechanism in the wall region, as revealed by the experimental investigation.

4.1. Description of the problem

The flow geometry was the same as the experimental set-up. The Cartesian coordinate system was used, with x, y and z denoting the streamwise, wall-normal and spanwise directions, respectively, and the reference point was chosen at the center of the spherical particle.

Although the flows, as investigated experimentally, were turbulent, steady laminar flow was assumed for the preliminary simulation studies. This was due to the fact that there are no models

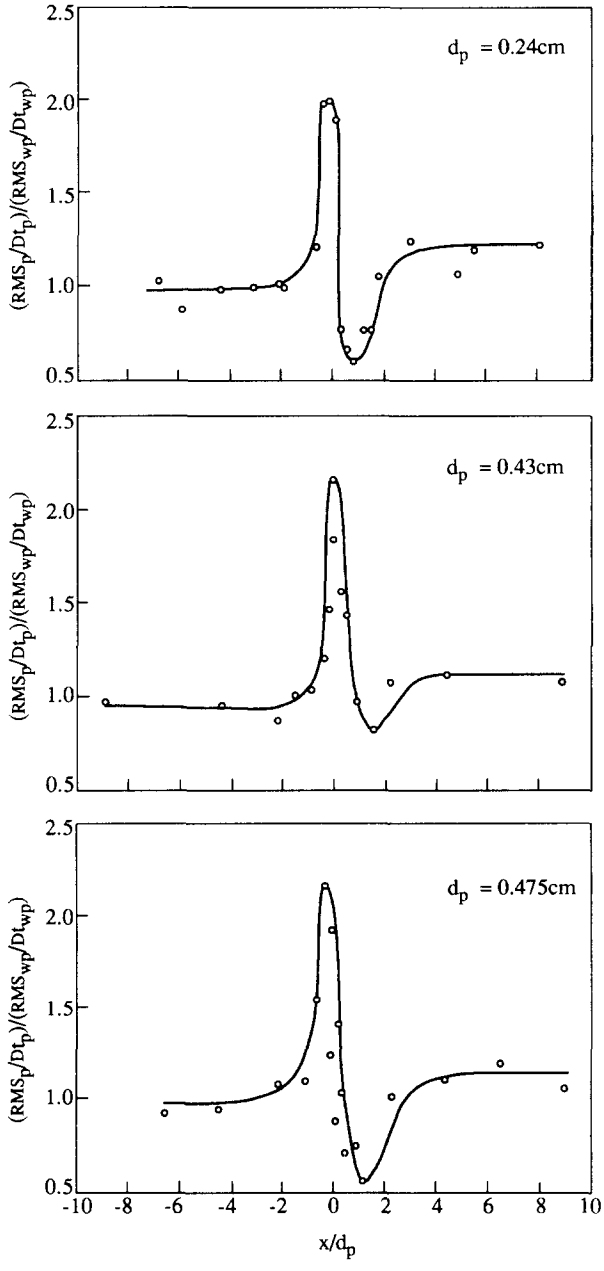

Figure 10. Variation of the relative RMS temperature vs the dimensionless distance x/d_p, $Re_h = 5150$.

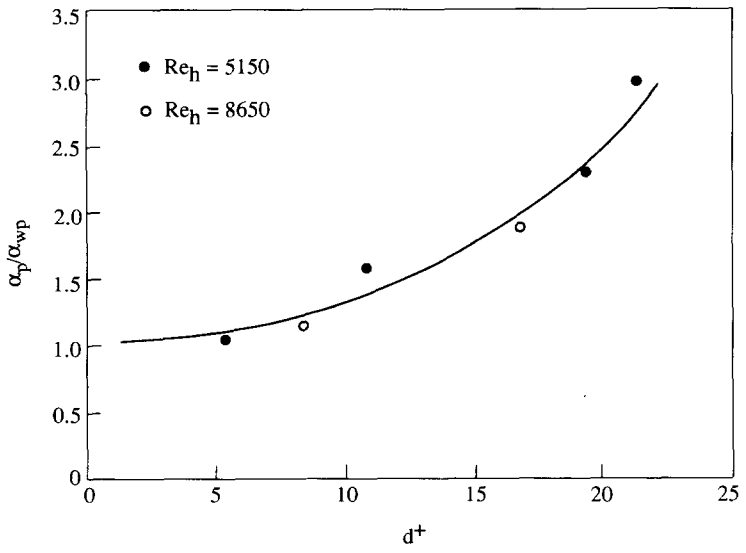

Figure 11. The variation of the maximal values of the local heat transfer coefficient α_p/α_{wp} vs the dimensionless particle diameter $d_p^+ = d_p u^*/\nu$.

available for turbulent flows which could properly represent this case, i.e. the flow field around a particle on the bottom of a flume, in the viscous and buffer regions of the wall. A proper mathematical description of such flows may be achieved by using direct numerical simulation, which is under investigation. Hence the numerical investigation based on laminar flow assumption also serves as the preliminaries of the DNS studies.

For a steady, incompressible, three-dimensional laminar flow in the Cartesian coordinates, the governing equations are very standard, hence they are not given here. The boundary conditions were the same as the experimental ones, except that the two side walls of the flume were treated as two symmetry planes. The particle was thermally conducting, and the continuity of heat flux was imposed on the surface of the particle as well as the no-slip conditions on all solid surfaces.

4.2. The grids and the numerical methods

The simulation was carried out by using Harwell code CFDS FLOW-3D release 3.2.1. The code provides a flexible framework of finite difference schemes and a body-fitted grid generation package with a multi-block structuring facility.

4.2.1. The grids. Twenty five blocks were used to construct the flow geometry so that the finer grids could be used where necessary in addition to a facility which may be used to generate grids of varying density. The grids used are illustrated as in figure 12. Due to the proportion of the particle in the whole set-up, only part of the grids surrounding the particle is shown. The particle was resolved by $6 \times 6 \times 6$ ($x \times y \times z$) grid points, and the typical grid spacings surrounding the particle ranged from 3.92×10^{-4} m to 7.83×10^{-4} m in both streamwise and spanwise directions and was 7×10^{-4} m in the wall-normal direction. A total of $62 \times 20 \times 32$ grid points were used for the whole flow domain.

It should be mentioned that, due to the technical problem of FLOW-3D, some grids between the base of the particle and the bottom wall could only be interpreted as solid instead of fluid. Hence the geometry there was not exactly the same as the experimental one. This discrepancy was judged minor for the present investigation.

4.2.2. Numerical methods. In the simulations, hybrid differencing was used; SIMPLEC was chosen to solve the pressure–velocity coupling, which is a modified form of the SIMPLE algorithm; the linearized momentum and energy equations were solved by using Stone's method; while the pressure correction equation was solved by using the preconditional conjugate gradients method. The numerical methods were first tested on a grid system, without particles, of grid spacings similar to the one described previously. The numerical solutions were found to be

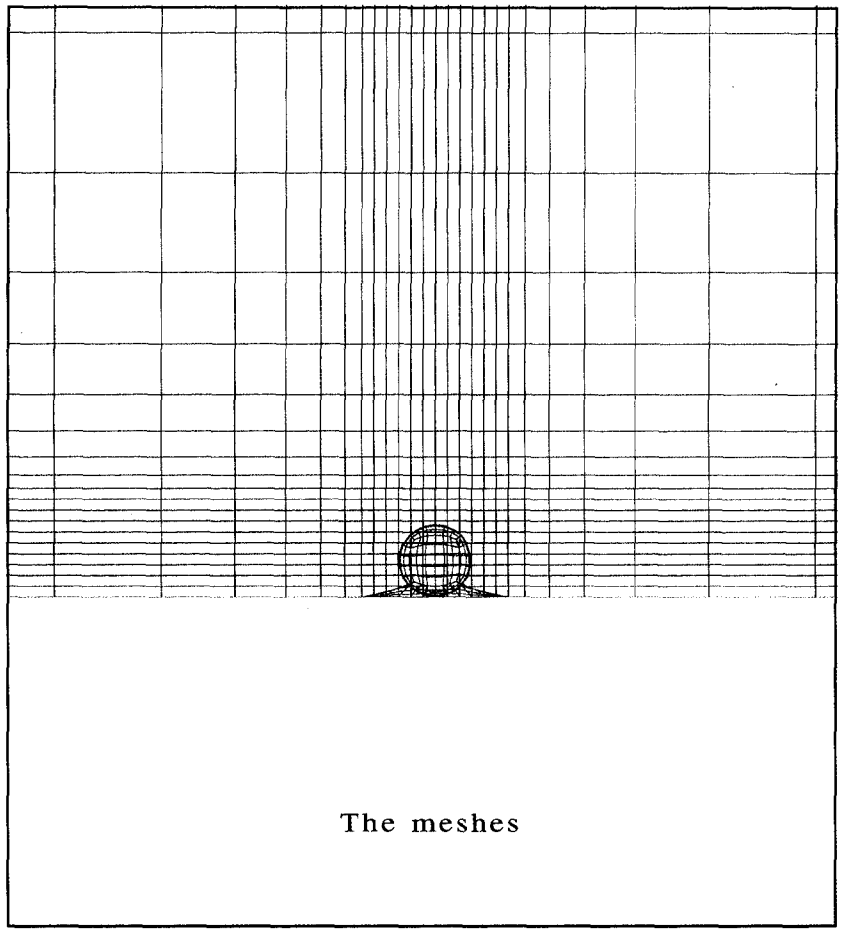

Figure 12. The spanwise view of the grids surrounding the particle.

satisfactory in comparison with the exact solutions of steady two-dimensional open channel flows (Lu & Hetsroni 1995).

4.3. *Simulation results and discussion*

Figure 13 illustrates the calculated wall temperature distribution around the particle. The flow is from the left to the right. The black straight lines are the inter-block boundaries reflecting the multi-block structure of the grids, while the circle is the projection of the particle onto the bottom of the flume. Since the calculation was performed for steady, thermally developing, laminar flow there is a general temperature gradient in the streamwise direction, except the areas that are under considerable influence of the particle, while the instantaneous experimental results, as shown in figure 2(b), exhibit the typical streaky structures associated with turbulence outside the particle influencing areas, and the temperature fluctuations overshadow the longitudinal temperature gradient, which is much smaller than the laminar gradient.

Despite the above, the basic pattern, as obtained by calculation, bears striking similarities to that of the experimental results, i.e. a cooler crescent area in front of the particle and a cooler tail in the wake of the particle with a smaller warmer area between the particle and the tail. This might indicate that the specific heat transfer pattern or the temperature pattern around the particle are, to a large degree, the consequences of the flow field or the flow pattern caused by the particle regardless of turbulence.

Figure 14(a), (b) and (c) shows the velocity field projected on the various cross-sections. It is clear from figure 14(a), which is an x–y plane, that the colder crescent area on the wall is a result of the in-rush of cooler fluid from the outer layers into the immediate vicinity of the wall, while figure 14(b) (a y–z plane, $6 \times d_p$ downstream of the particle) demonstrates two counter-rotating streamwise vortices in the wake of the particle, which give rise to the cooler tail area on the wall. Figure 14(c) (an x–z plane) shows that the smaller warmer area right behind the particle is caused by two smaller vortices rotating in a way which always entrains warmer fluid into this area.

In figure 15(a) and (b), both numerical and experimental values of the ratio of the heat transfer coefficient with the particle to that without particles, along the streamwise center line on the bottom wall, are presented. It is very interesting to see that the numerical results agree reasonably well with the experimental ones, though the location of the maximum ratio calculated shifts slightly upstream compared with the experimental one due to the technical problem regarding the interpretation of some grids between the base of the particle and the bottom wall, as mentioned previously.

The close agreement between the numerical and the experimental results shown as in figure 15(a) and (b) may indicate that the relative variation of heat transfer characteristics, due to a particle, depends on the flow pattern regardless of the turbulence, though the turbulent components do contribute to the absolute heat transfer process. Both numerical and experimental results also indicate that the particle influencing regions are within about 1–2 particle diameters from the center of the particle except the wake region which may drag to about 6–8 particle diameters downstream of the center.

5. DISCUSSION AND SUMMARY

The I.R. technique was used to study the effect of a particle on the local heat transfer coefficient from a heated wall to a fluid. The measurements of the temperature fields with the particle and without it have shown that the local heat transfer coefficient increases by 1.5 to 3 times for a particle of the order of $d_p^+ = 10$ to 25. A general decrease in the wall temperature was observed in the region under and in front of the particle and in its wake. We did not note any effect of the particle material (steel, glass, polystyrene), and the dimensionless diameter $d_p^+ = d_p u^*/\nu$ and the geometry are probably the only parameters of this phenomenon.

We also studied the temperature fluctuations of the heated foil at the bottom of a flume. We assume that these fluctuations are related to the bursting process in the turbulent flow. The measurements of the bursting period, by means of VITA technique, indicated a value of the dimensionless time between the bursts of $\Delta\tau^+ \cong 290$ which corresponds very well to the data of Blackwelder & Haritonidis (1983), Willmarth & Sharma (1984) and Lu & Smith (1991).

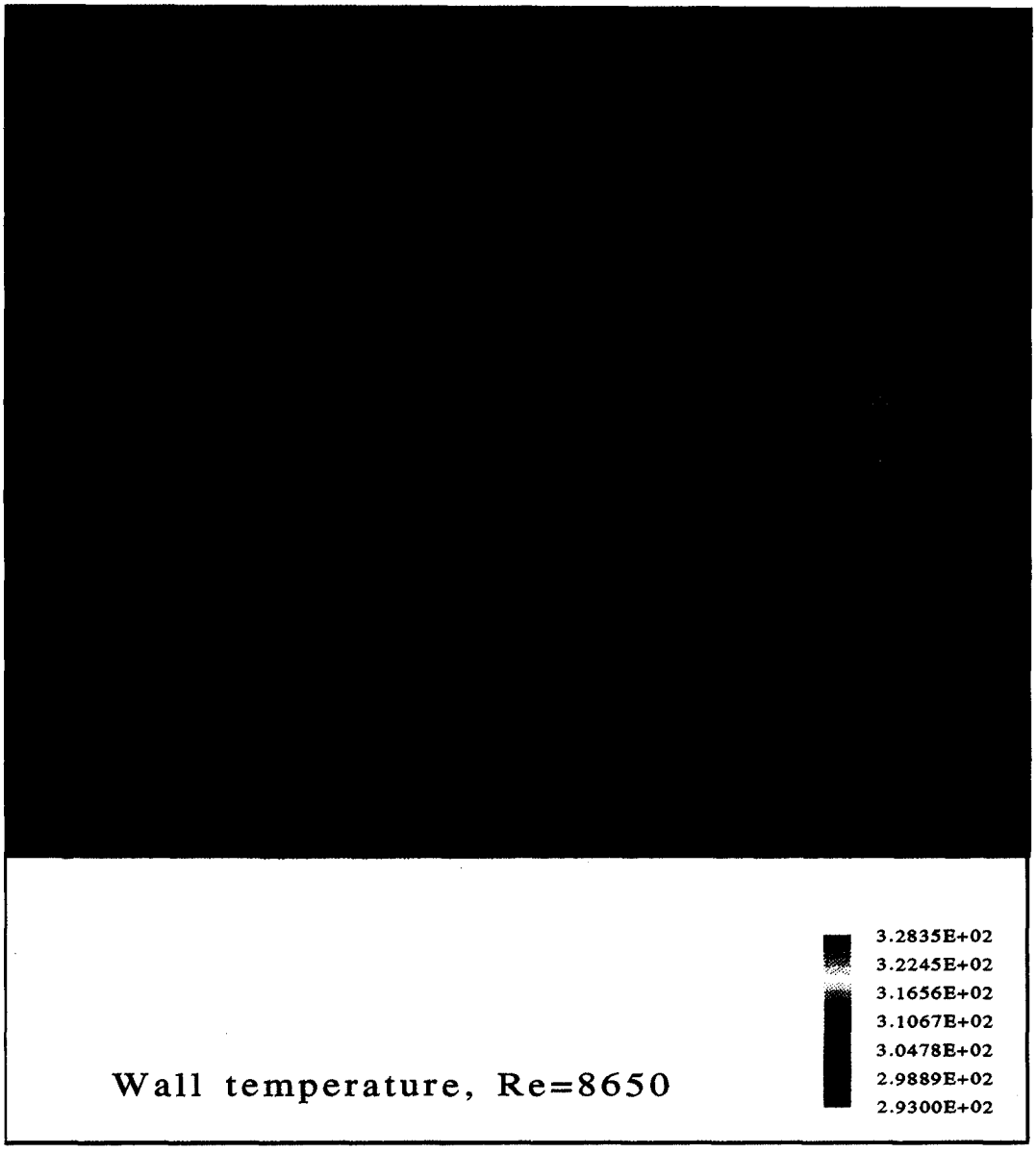

Figure 13. The wall temperature, Re = 8650 and $d_p = 4.75$ mm.

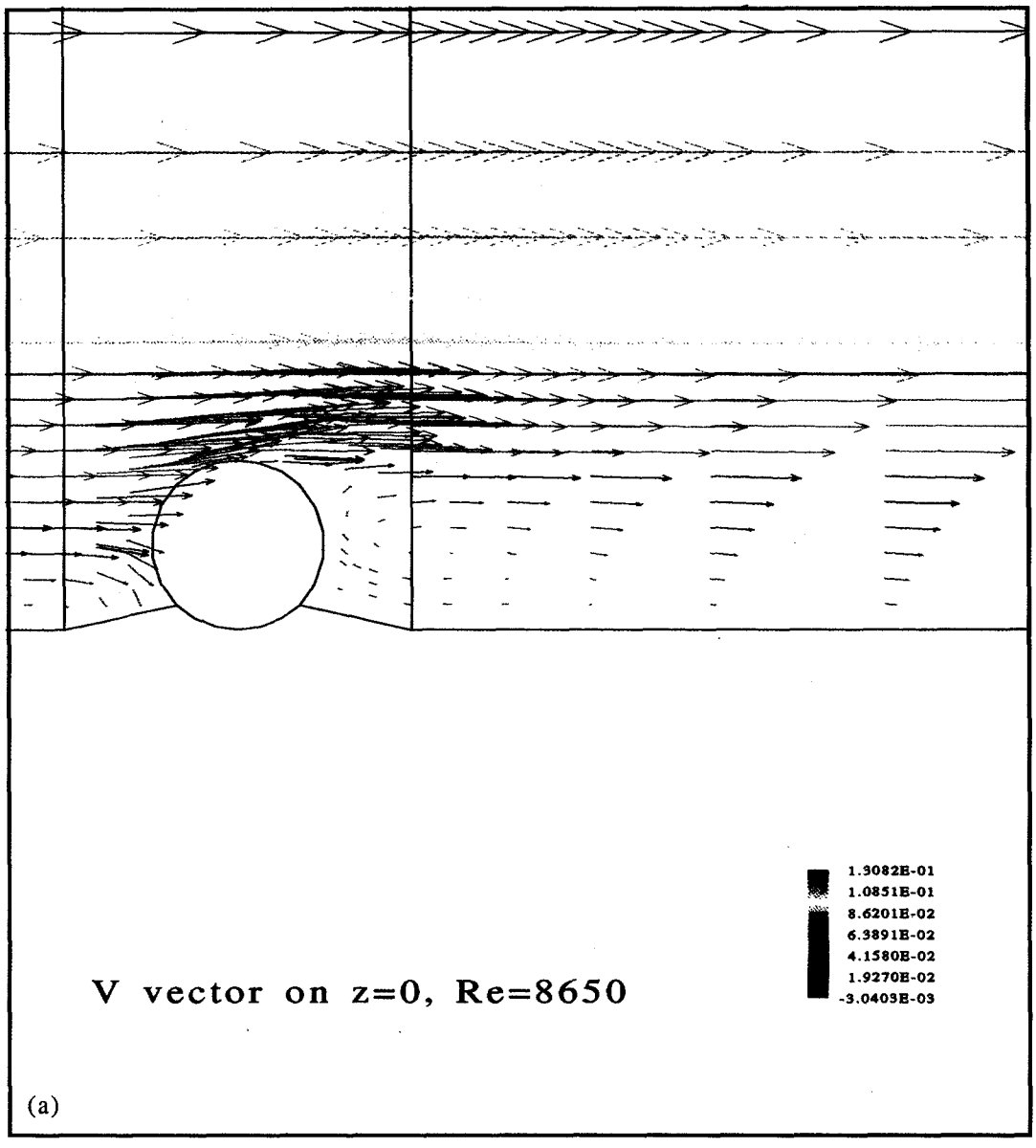

Figure 14(a) *Caption on p. 981*

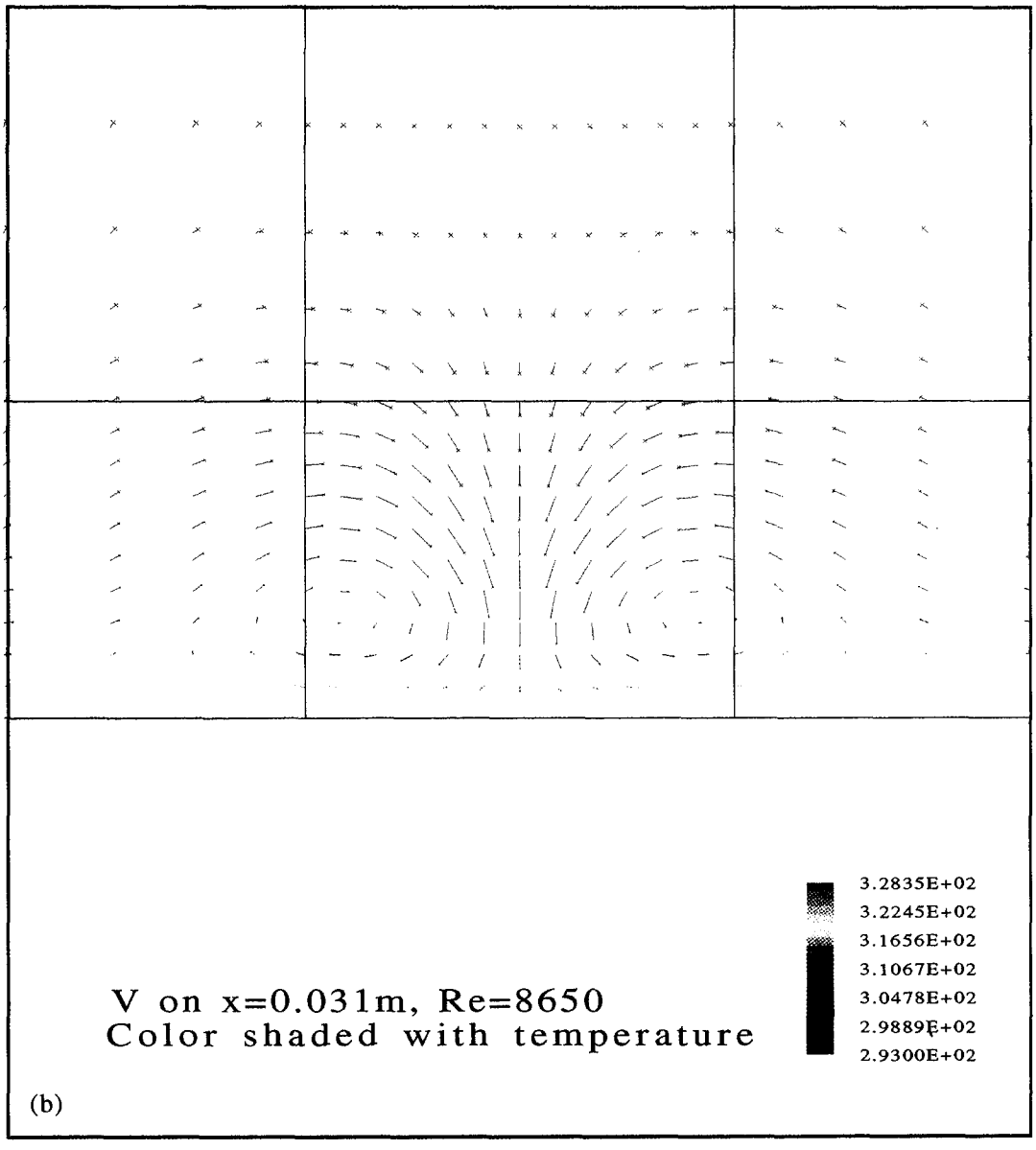

Figure 14(b) *Caption on p. 981*

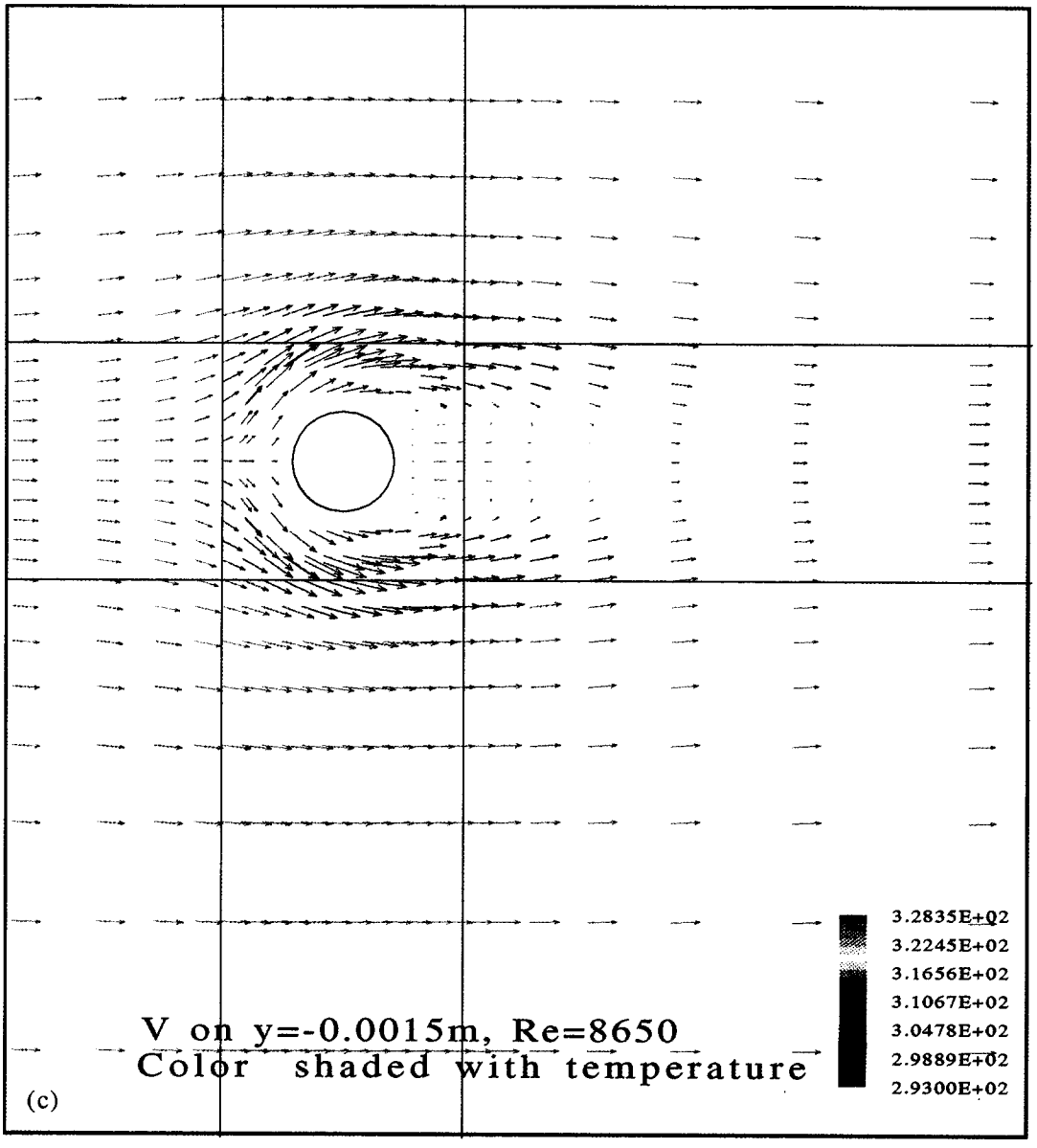

Figure 14(c)

Figure 14. The velocity field as projected onto various planes Re = 8650, d_p = 4.75 mm (a) $z = 0$ plane, (b) $x = 0.031$ m plane and (c) $y = -0.0015$ m plane.

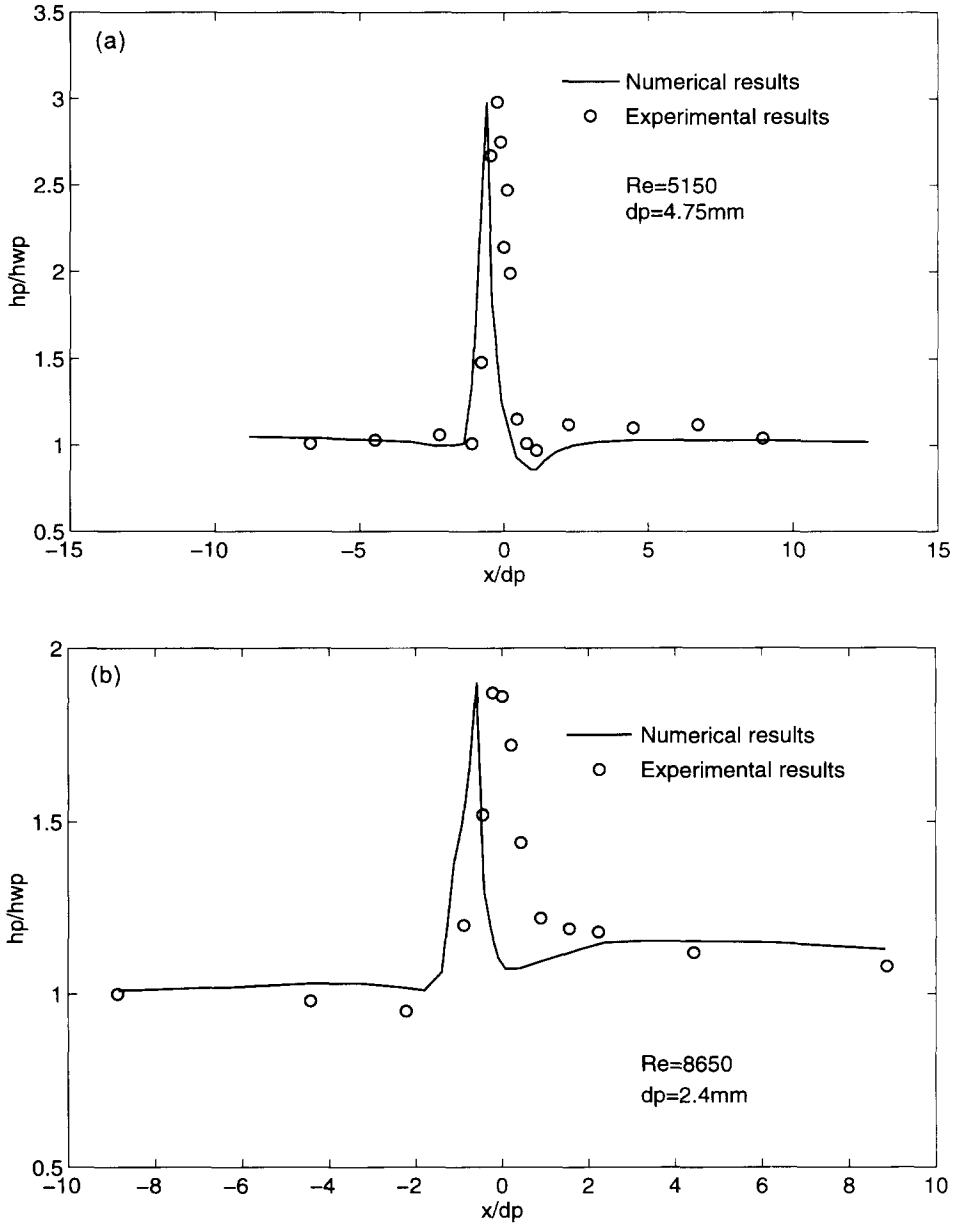

Figure 15. The relative variation of heat transfer coefficient—comparison between numerical and experimental results (a) Re = 5150, d_p = 4.75 mm and (b) Re = 8650, d_p = 2.4 mm.

It is possible that increasing the bursting period means decreasing the turbulence level in the flow near the particle. Together with the decrease in RMS level, this most likely indicates that the heat transfer enhancement is governed by some other mechanism, such as a change in the velocity profile near the wall. The similarity between the curves $\alpha_p/\alpha_{wp} = f(x/d_p)$ and $(RMS_p/Dt_p)/(RMS_{wp}/Dt_{wp}) = f(x/d_p)$ also may indicate that the heat transfer coefficient is linked with the temperature change near the particle. Indeed, the considerable heat transfer enhancement in this case may be explained by the considerable decrease in the value of the temperature difference Dt_p between the wall temperature and the bulk temperature of the liquid, since the value of (Dt_{wp}/RMS_{wp}). RMS_p does not increase (figures 8 and 9). This decrease in the value Dt_p is related to an in-rush of cold fluid from the mainstream. The numerical computations of the velocity profiles near the particle indicate clearly that there is an in-rush of cold fluid from the mainstream to the wall region. This in-rush occurs mainly in front of the particle and some in its wake.

Acknowledgements—This research was supported by a United States–Israel Binational Science Foundation Grant No. 90-00428/1, by the Basic Research Foundation administered by the Israel Academy of Science and Humanities, The Ministry of Science and the Arts, State of Israel, the Technion V.P.R. Fund–Israel–Mexico Energy Research Fund and by the Fund for the Promotion of Research at the Technion. R. R. is partially supported by the Center for Absorption in Science, Ministry of Immigrants Absorption, State of Israel. D. M. L. is supported by a grant from the Israel Council of Higher Education.

REFERENCES

Blackwelder, R. F. & Eckelmann, H. 1978 In *Structure and Mechanism of Turbulence* (Edited by Fiedler, H.), Lecture Notes in Physics, p. 190. Springer, Berlin.

Blackwelder, R. F. & Haritonidis, J. H. 1983 Scaling of the bursting frequency in turbulent boundary layers. *J. Fluid Mech.* **132,** 87–103.

Blackwelder, R. F. & Kaplan, R. E. 1976 On the wall structure of the turbulent boundary layer. *J. Fluid Mech.* **76,** 89–112.

Chen, C. P. & Blackwelder, R. F. 1978 The large-scale motion in a turbulent boundary layer: a study using temperature contamination. *J. Fluid Mech.* **89,** 1–31.

Eaton, J. K. & Fessler, J. R. 1994 Preferential concentration of particles by turbulence. *Int. J. Multiphase Flow* **20,** 169–210.

Fitzpatrick, J. A., Lambert, B. & Murray, D. B. 1992 Measurements in the separation region of a gas–particle cross flow. *Exp. Fluids* **12,** 329–341.

Grass, A. J., Stuart, R. G. & Mansour-Tehrany, M. 1991 Vortical structures and coherent motion in turbulent flow over smooth and rough boundaries. In *Turbulent Flow Structure Near Walls.* pp. 35–65. Royal Society, London .

Han, K. S., Sung, H. J. & Chung, M. K. 1991 Analysis of heat transfer in a pipe carrying two-phase gas–particle suspension. *Int. J. Heat Mass Transfer* **34,** 69–78.

Hatziavramidis, D. T. & Hanratty, T. Y. 1979 The representation of the viscous wall region by a regular eddy pattern. *J. Fluid Mech.* **95,** 655–679.

Hasegawa, S., Echigo, R., Kanemaru, K., Ichimiya, K. & Sanui, M. 1983 Experimental study of forced convective heat transfer of flowing gaseous solid suspension at high temperature. *Int. J. Multiphase Flow* **9,** 131–145.

Hetsroni, G. 1989 Particle–turbulence interaction. *Int. J. Multiphase Flow* **15,** 735–746.

Hetsroni, G. & Rozenblit, R. 1994 Heat transfer to liquid–solid mixture in a flume. *Int. J. Multiphase Flow* **20,** 671–689.

Jepson, G., Poll, A. & Smith, W. 1963 Heat transfer from gas to wall in a gas–solids transport line. *Trans. Inst. Chem. Egrs* **41,** 207–211.

Kaftori, D., Hetsroni, G. & Banerjee, S. 1992 Modulation of turbulence structures by particles. *AIChE Meeting*, 1–6 November, Miami Beach, FL.

Kaftori, D., Hetsroni, G. & Banerjee, S. 1994 Funnel-shaped vortical structures in wall turbulence. *Phys. Fluids A* **6,** 3035–3050.

Kim, H. T., Kline, S. J. & Reynolds, W. C. 1971 The production of turbulence near a smooth wall in a turbulent boundary layer. *J. Fluid Mech.* **50,** 133–160.

Kline, S. J., Reynolds, W. C., Schraub, F. A. & Runstandler, P. W. 1967 The structure of turbulent boundary layers. *J. Fluid Mech.* **70,** 741–773.

Komori, S., Murakami, Y. & Ueda, H., 1989 The relationship between surface-renewal and bursting motions in an open-channel flow. *J. Fluid Mech.* **203,** 103–123.

Lu, D. M. & Hetsroni, G. 1995 Direct numerical simulation of turbulent channel flow with passive heat transfer. *Int. J. Heat Mass Transfer.* In press.

Lu, L. J. & Smith, C. R. 1991 Use of quantitative flow visualization data for examination of spatial–temporal velocity and burst-type characteristics in a turbulent boundary layer. *J. Fluid Mech.* **232,** 303–340.

Lu, S. S. & Willmarth, W. W. 1973 Measurement of structure of the Reynolds stress in a turbulent boundary layer. *J. Fluid Mech.* **60,** 481–511.

Luchik, T. S. & Tiederman, W. G. 1987 Timescale and structure of ejections and bursts in turbulent channel flow. *J. Fluid Mech.* **174,** 529–552.

Murray, D. B. 1994 Local enhancement of heat transfer in a particulate cross flow. *Int. J. Multiphase Flow* **20,** 493–513.

Murray, D. B. & Fitzpatrick, J. A. 1991 Heat transfer in a staggered tube array for a gas–solid suspension flow. *Trans. ASME, J. Heat Transfer* **113,** 865–873.

Pedinotti, S., Mariotti, G. & Banerjee, S. 1992 Direct numerical simulation of particle behaviour in the wall region of turbulent flows in horizontal channels. *Int. J. Multiphase Flow* **18,** 927–941.

Plass, L. & Molerus, O. 1974 Simultane Wärmeübergangs-und Druckverlustmessungen an Feststoff/Flüssigkeits-Suspensionen im Übergangsbereich vom homogenen zum heterogenen Suspensions-transport. *Chem. Ing. Tech.* **46,** 355.

Rashidi, M. & Banerjee, S. 1988 Turbulence structure in free surface channel flows. *Phys. Fluids* **31,** 2491–2503.

Rashidi, M., Hetsroni, G. & Banerjee, S. 1990 Particle–turbulence interaction in a boundary layer. *Int. J. Multiphase Flow* **16,** 935–949.

Rogers, C. B. & Eaton, J. K. 1989 The interaction between dispersed particles and fluid turbulence in a flat plate turbulent boundary layer in air. Report MD-52, Stanford University, CA.

Subramanian, C. S., Rajagopalan, S., Antonia, R. A. & Chambers, A. J. 1982 Comparison of conditional sampling and averaging techniques in a turbulent boundary layer. *J. Fluid Mech.* **123,** 335–362.

Wallace, J. M., Eckelman, H. & Brodkey, R. S. 1972 The wall region of turbulent shear flow. *J. Fluid Mech.* **54,** 39–48.

Wilkinson, G. T. & Norman, J. R. 1967 Heat transfer to a suspension of solids in a gas. *Trans. Inst. Chem. Engrs* **45,** 314–318.

Willmarth, W. W. & Sharma, L. K. 1984 Study of turbulent structure with hot wires smaller than the viscous length. *J. Fluid Mech.* **142,** 121–149.

Zisselmar, R. & Molerus, O. 1979 Investigation of solid–liquid pipe flow with regard to turbulence modification. *Chem. Engng J.* **18,** 233–239.